

Gouy phase and quantum interference with cross-Wigner functions for matter-waves

Lucas S. Marinho ^{1,2,*}, Pedro R. Dieguez ³, Carlos H. S. Vieira ^{4,†} and Irismar G. da Paz ^{1,‡}

¹*Departamento de Física, Universidade Federal do Piauí,*

Campus Ministro Petrônio Portela, 64049-550, Teresina, PI, Brazil

²*Departamento de Física, Universidade Federal de Pernambuco, 50670-901 Recife, Pernambuco, Brazil*

³*International Centre for Theory of Quantum Technologies,*

University of Gdańsk, Jana Bazynskiego 8, 80-309 Gdańsk, Poland

⁴*Centro de Ciências Naturais e Humanas, Universidade Federal do ABC,*

Avenida dos Estados 5001, 09210-580 Santo André, São Paulo, Brazil

The Gouy phase is essential for accurately describing various wave phenomena, ranging from classical electromagnetic waves to matter waves and quantum optics. In this work, we employ phase-space methods based on the cross-Wigner transformation to analyze spatial and temporal interference in the evolution of matter waves characterized initially by a correlated Gaussian wave packet. First, we consider the cross-Wigner of the initial function with its free evolution, and second for the evolution through a double-slit arrangement. Different from the wave function which acquires a global Gouy phase, we find that the cross-Wigner acquires a Gouy phase difference due to different evolution times. The results suggest that temporal like-Gouy phases are important for an accurate description of temporal interference. Furthermore, we propose a technique based on the Wigner function to reconstruct the cross-Wigner from the spatial intensity interference term in a double-slit experiment with matter waves.

I. INTRODUCTION

Gouy phase is a wave phenomenon that appears when waves are confined transversely to their propagation direction, such as in the case of lens focusing and diffraction through slits. It was first observed for classical light waves [1, 2] and it has been recently investigated for the transverse confinement of matter waves [3–6]. The Gouy phase and its properties have been extensively studied [7–10], and the acquired phase is known to depend on the type of transversal confinement and the geometry of the waves. For instance, line-focusing a cylindrical wave propagating from $-\infty$ to $+\infty$ yields a Gouy phase of $\pi/2$, while point-focusing a spherical wave in the same interval yields a Gouy phase of π [11]. Gaussian matter wave packets diffracting through small apertures generate a Gouy phase of $\pi/4$ [12]. Experiments were performed with acoustic and water waves [13–15], surface plasmon-polaritons with non-Gaussian spatial properties [16], focused cylindrical phonon-polariton wave packets in LiTaO₃ crystals, and for Bose-Einstein condensates and electron waves [17–20]. Interestingly, the effects of the quantum Gouy phase was also verified with the evolution of two-photon states [21].

Applications, such as in evaluating the resonant frequencies in laser cavities [22], in phase-matching in strong-field and high-order harmonic generation [23–25], and in describing the spatial profile of laser pulses with high repetition rate [26] was shown to be feasible. In addition, an extra Gouy phase appears in optical and

matter waves depending on the orbital angular momentum's magnitude [18, 19, 27, 28]. In recent work, it was found that the Gouy phase may cause nonlocal effects that modify the symmetries of self-organization in atomic systems [29]. This phase may also be useful in communication and optical tweezers using structured light [30]. Gouy phases in matter waves also display potential applications and can be used in mode converters in quantum information systems [31], in the generation of singular electron optics [20] and in the study of non-classical (exotic or looped) paths in interference experiments [32].

Since the Gouy phase of matter waves is directly related to position-momentum correlations [4, 33], we propose in this work to investigate the role of the Gouy phase employing initial position-momentum correlations by using the cross-Wigner transform to analyze the temporal evolution of matter waves. The cross-Wigner transform has been employed in different contexts such as signal processing [34, 35], and quantum measurement theory [36, 37]. In signal processing, for instance, it is used to analyze the time-frequency content of signals as it allows one to analyze signals in both the time and frequency domains simultaneously [34, 35]. In quantum theory, the cross-Wigner was employed as an analog of the two-state vector formalism [38] for continuous variables [37] and to derive the weak values of an observable from a complex quasi-probability distribution associated with it [36]. Its physical interpretation showed to be that of an interference term in the Wigner distribution of the sum of two different wave functions. Then, the cross-Wigner transform is a suitable formalism to work with spatial and temporal interference of quantum states.

Temporal interference emerges as an alternative approach to scrutinize entanglement across different degrees of freedom, such as time-energy entanglement. For instance, the pioneering Franson interferometry [39] intro-

* lucas.marinho@ufpi.edu.br

† carloshsv09@gmail.com

‡ irismarpaz@ufpi.edu.br

duces a novel experimental test for local hidden-variable theories centered on time interference, and visibility greater than 70.7% for this setup is known to indicate a violation of a Bell-type inequality, and recent experimental work has reached $96 \pm 1\%$ without background subtraction for entanglement photon pairs generated by spontaneous parametric down-conversion [40]. The temporal analog of a double-slit experiment for light waves has also been observed [41], showing a clear signature of spectral oscillations for time-diffracted light and an inversely proportional relation between slit separation and period of oscillations. For experiments with matter wave packets, the same type of effect was observed, demonstrating a one-by-one detection scheme, allowing us to visualize the buildup of the quantum interference pattern of single-photoelectrons which stochastically arrive at the detector plane [42].

The cross-Wigner transform is used here to access the temporal interference in two different scenarios (with and without double-slit arrangements) to understand the role of the Gouy phase in temporal interference. The manuscript is organized as follows. In section II, we review the cross-Wigner formalism. In section III, we introduce our contribution by constructing the cross-Wigner transformation between an initial Gaussian wave packet and its corresponding free-evolved state. In section IV, we introduce a double-slit setup to understand how spatial interference coming from the diffraction in the slits relates to the temporal interference captured by the Gouy phase through the cross-Wigner distribution. Finally, we propose in sec. IV A an approach to reconstruct the cross-Wigner in a double-slit experiment from the intensity interference term. In section V we present our conclusions.

II. CROSS-WIGNER FUNCTION

In this section, we review the cross-Wigner transform [36], a generalization of the Wigner function for pre and post-selected ensembles. In the quantum phase space, the Wigner distribution

$$W(x, k) = \frac{1}{2\pi} \int dy e^{-iky} \psi^*(x + y/2) \psi(x - y/2), \quad (1)$$

describes the state $\psi(x)$ of a given system, and it is normalized over all phase space. Also, it provides the marginal probability distribution for momentum $|\phi(k)|^2 = \int dx W(x, k)$, and position $|\psi(x)|^2 = \int dk W(x, k)$ of a system.

The cross-Wigner transform of two functions can be defined as

$$\mathcal{CW}_{\psi, \phi}(x, k) \equiv \frac{1}{2\pi} \int dy e^{-iyk} \phi^*(x + y/2) \psi(x - y/2), \quad (2)$$

where ϕ and ψ are wave functions. Interestingly, the appearance of interference terms are described by the

cross-Wigner transform

$$W_{\psi+\phi}(q, p) = W_{\psi} + W_{\phi} + 2\text{Re}[\mathcal{CW}_{\psi, \phi}], \quad (3)$$

where W_{ψ} (W_{ϕ}) is the Wigner function of state ψ (ϕ), respectively, and $\text{Re}[\mathcal{CW}_{\psi, \phi}]$ is the real part of cross-Wigner function between ψ and ϕ , represents an interference term in the Wigner function of the superposition $W_{\psi+\phi}$. Also, note that the cross-Wigner transform $\mathcal{CW}_{\psi, \phi}(x, k)$ reduces to the familiar Wigner distribution when $\phi = \psi$.

The cross-Wigner transform satisfies the following properties

$$\int \mathcal{CW}_{\psi, \phi}(x, k) dk = \phi^*(x) \psi(x) \quad (4)$$

and

$$\int \mathcal{CW}_{\psi, \phi}(x, k) dx = F \phi^*(k) F \psi(k), \quad (5)$$

where

$$F \psi(k) = \frac{1}{\sqrt{2\pi}} \int dx e^{-ikx} \psi(x) \quad (6)$$

is the Fourier transform of ψ . Also, one can check that

$$\iint \mathcal{CW}_{\psi, \phi}(x, k) dx dk = \langle \phi | \psi \rangle. \quad (7)$$

In the following, we explore the cross-Wigner function under free evolution to observe how the Gouy phase appears in that context.

III. CROSS-WIGNER FUNCTION AND GOUY PHASE IN FREE EVOLUTION

In this section, we show that while the wave function acquires a global Gouy phase, the cross-Wigner acquires a relative Gouy phase if we consider the transformation between the initial and a freely evolved state.

Consider as the initial state the following correlated Gaussian state of transverse width σ_0

$$\psi_0(x_i) = \frac{1}{\sqrt{\sigma_0 \sqrt{\pi}}} \exp \left[-\frac{x_i^2}{2\sigma_0^2} + \frac{i\gamma x_i^2}{2\sigma_0^2} \right]. \quad (8)$$

The initial correlation will be represented by the real parameter γ which can take values in the interval $-\infty < \gamma < \infty$ [43, 44].

The wave function at t is given by [45]

$$\psi(x, t) = \int_{-\infty}^{\infty} dx_i G(x, t; x_i, 0) \psi_0(x_i), \quad (9)$$

where

$$G(x, t; x_i, 0) = \sqrt{\frac{m}{2\pi i \hbar t}} \exp \left[\frac{im(x - x_i)^2}{2\hbar t} \right]. \quad (10)$$

The kernel $G(x, t; x_i, 0)$ is the free nonrelativistic propagator for a particle of mass m . After some algebraic manipulation, we obtain

$$\psi(x, t) = \frac{1}{\sqrt{b(t)\sqrt{\pi}}} \exp\left(-\frac{x^2}{2b(t)^2}\right) \exp\left(\frac{imx^2}{2\hbar r(t)} + i\mu(t)\right) \quad (11)$$

where

$$b(t) = \frac{\sigma_0}{\tau_0} [t^2 + \tau_0^2 + 2t\tau_0\gamma + t^2\gamma^2]^{\frac{1}{2}}, \quad (12)$$

$$r(t) = \frac{(t^2 + \tau_0^2 + 2t\tau_0\gamma + t^2\gamma^2)}{[t(1 + \gamma^2) + \gamma\tau_0]}, \quad (13)$$

and

$$\mu(t) = -\frac{1}{2} \arctan\left(\frac{t}{\tau_0 + \gamma t}\right). \quad (14)$$

Here, $b(t)$ is the beam width, $r(t)$ is the radius of curvature of the wave fronts and $\mu(t)$ is the Gouy phase for the free propagation. The parameter $\tau_0 = m\sigma_0^2/\hbar$ is one intrinsic time scale which essentially corresponds to the time at which the distance of the order of the wave packet extension is traversed with a speed corresponding to the dispersion in velocity. It is viewed as a characteristic time for the ‘‘aging’’ of the initial state [45, 46], since it is a time from which the evolved state acquires distinguishable properties from the initial state.

Now, we calculate the cross-Wigner between the initial state and the state at t , as follows

$$CW_{\psi, \psi_0}(x, k) = \frac{1}{2\pi} \int_{-\infty}^{\infty} dy e^{-iky} \psi^*\left(x + \frac{y}{2}\right) \psi_0\left(x - \frac{y}{2}\right). \quad (15)$$

After some algebraic manipulation we obtain for its real and imaginary parts, respectively, the following results

$$\text{Re}[CW]_{\psi, \psi_0}(x, k) = N e^{-a_1 x^2} e^{-a_3 k^2} e^{a_5 k x} \cos(\phi), \quad (16)$$

$$\text{Im}[CW]_{\psi, \psi_0}(x, k) = N e^{-a_1 x^2} e^{-a_3 k^2} e^{a_5 k x} \sin(\phi), \quad (17)$$

where

$$\phi = a_2 x^2 + a_4 k^2 + a_6 k x + \Delta\mu, \quad (18)$$

and

$$\Delta\mu = \xi(t) - \mu(t) \quad (19)$$

with

$$\xi(t) = -\frac{1}{2} \arctan\left(\frac{\frac{m}{2\hbar r} - \frac{\gamma}{2\sigma_0^2}}{\frac{1}{2b^2} + \frac{1}{2\sigma_0^2}}\right). \quad (20)$$

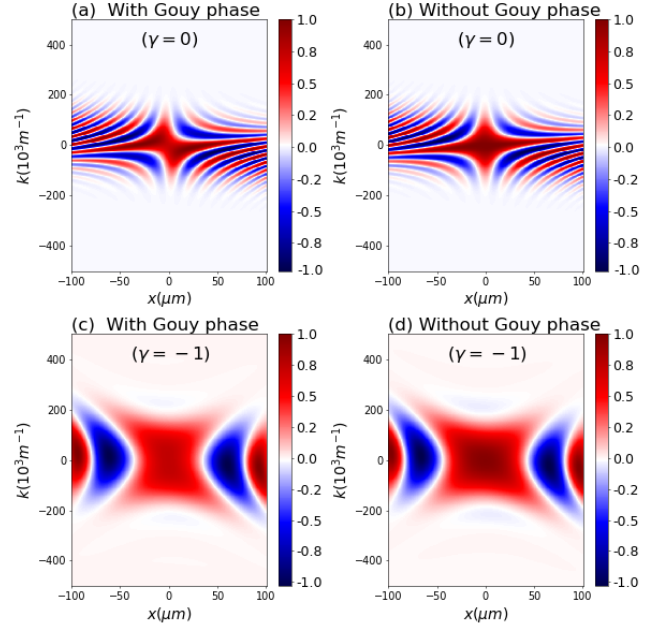


FIG. 1. Real part of the normalized cross-Wigner ($\text{Re}[CW]_{\psi, \psi_0}$) as a function of x and k for $t = 50$ ms and $\gamma = 0$ in (a) and (b), while for (c) and (d) we used $\gamma = -1$. In (a) and (c), we consider the Gouy phase difference, but in (b) and (d), we do not consider it. From these plots, it is evident the importance of the Gouy phase in this cross-Wigner formalism for an accurate and complete description of the quantum state. We have similar results for the imaginary component.

Here, $\Delta\mu$ is the cross-Wigner Gouy phase difference for the free evolution. The parameters N and a_i ($i = 1, \dots, 6$) are given in Appendix B.

In the following, we consider a wavefunction for neutrons with $m = 1.67 \times 10^{-27}$ kg, $\sigma_0 = 7.8 \mu\text{m}$. In Fig. 1, we show the real part of the normalized cross-Wigner from eq.(16) as a function of x and k for $t = 50$ ms and two different values of γ . In Fig. 1(a) and (b), we consider $\gamma = 0$, while for Fig. 1(c) and (d), we used $\gamma = -1$. In Fig. 1(a) and (c), we consider the Gouy phase difference, but in Fig. 1(b) and (d), we do not consider it. At this point, the importance of the Gouy phase in this cross-Wigner formalism for an accurate and complete description of the quantum state becomes evident. Here, the Gouy phase difference results from the fact that the cross-Wigner is calculated for wave functions at different times, i.e., $\psi(x, t)$ at the time $t > 0$ and ψ_0 at the time $t = 0$.

We show, in Fig. 2, the normalized cross-Wigner from eq.(16) between the initial state and the state at the time t as a function of x and t for $k = 0$ and $\gamma = 0$. We can see a cross-Wigner’s peak located around $(x = 0, t = 0)$, indicating that this is the region where there is greater overlap between $\psi(x, t)$ and $\psi_0(x)$. Nevertheless, the overlapping decreases at high t values, which reduces the cross-Wigner function.

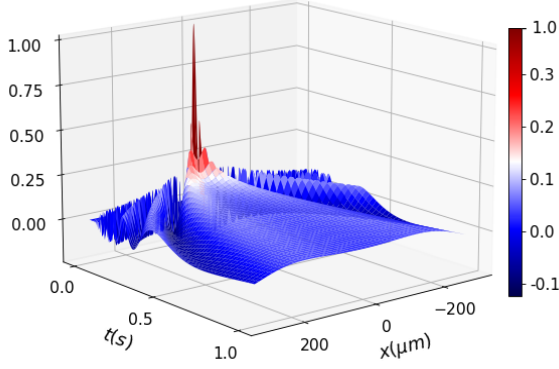


FIG. 2. Normalized cross-Wigner real part ($\text{Re}[CW]_{\psi, \psi_0}$) as a function of x and t for $k = 0$ and $\gamma = 0$. Around the ($x = 0, t = 0$), exists one maximum indicating that in this region there is greater overlap between $\psi(x, t)$ and $\psi_0(x)$.

IV. CROSS-WIGNER FUNCTION AND GOUY PHASE IN THE DOUBLE-SLIT EXPERIMENT

Consider a classical double-slit experiment with an initially correlated Gaussian wavepacket given by eq. (8). Assume that such coherent correlated Gaussian wavepacket is produced in the source S and propagates during a time t before arriving at a double-slit which splits it into two Gaussian wavepackets. After crossing the grid, the wavepackets propagate during a time τ before arriving at detector D in the detection screen. In this model, we realize quantum effects only in x -direction as we can assume that the energy associated with the momentum of the particles in the z -direction is high enough such that the momentum component p_z is sharply defined, i.e., $\Delta p_z \ll p_z$. Then we can consider a classical behavior in this direction at velocity v_z , and hence we can write $z = v_z t$ [32]. The sketch of this model is presented in Fig. 3.

The wavefunctions at the right 1(+) and left slit 2(-) are given by [45]

$$\psi(x, t, \tau) = \int_{-\infty}^{\infty} dx_j \int_{-\infty}^{\infty} dx_i G(x, t + \tau; x_j, t) \times F(x_j \pm d/2) \psi(x_j, t), \quad (21)$$

where

$$G(x, t + \tau; x_j, t) = \sqrt{\frac{m}{2\pi i \hbar \tau}} \exp\left[\frac{im(x - x_j)^2}{2\hbar \tau}\right], \quad (22)$$

and

$$F(x_j \pm d/2) = \frac{1}{\sqrt{\beta\sqrt{\pi}}} \exp\left[-\frac{im(x_j \pm d/2)^2}{2\beta^2}\right]. \quad (23)$$

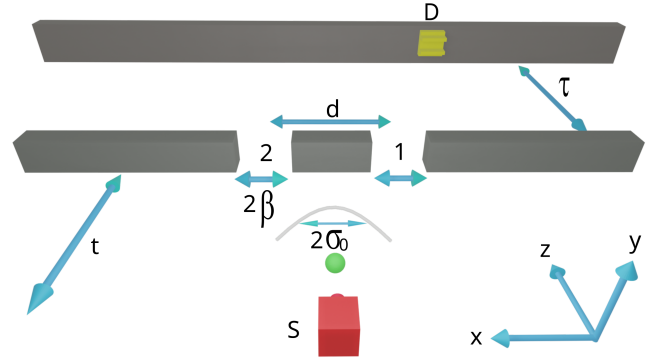


FIG. 3. Sketch of the double-slit experiment. The source S produces a correlated Gaussian wavepacket with the transverse width σ_0 . The wavepacket propagates during a time t before attaining the double-slit and during a time τ from the double-slit to the detector D in the screen of detection. The slit transmission functions are taken to be Gaussian of width β and separated by a distance d .

$F(x_j \pm d/2)$ describes the double-slit transmission functions which are taken to be Gaussians of width β separated by a distance d . The parameter γ ensures that the initial state is correlated. In fact, we obtain for the initial state $\psi_0(x_i)$ that the uncertainty in position is $\sigma_{xx} = \sigma_0/\sqrt{2}$, whereas the uncertainty in momentum is $\sigma_{pp} = (\sqrt{1 + \gamma^2})\hbar/\sqrt{2}\sigma_0$ and the σ_{xp} correlations is $\sigma_{xp} = \hbar\gamma/2$. For $\gamma = 0$ we have a simple uncorrelated Gaussian wavepacket with $\sigma_{xp} = 0$. To obtain analytic expressions for the wavefunction, Wigner and Cross-Wigner functions in the screen of detection, we use a Gaussian transmission function instead of a top-hat transmission one because both a Gaussian transmission function represents a good approximation to the experimental reality and it is mathematically simpler to treat than a top-hat transmission function.

The wavefunction that passed through slit 1(+)

$$\psi_1(x, t, \tau) = \frac{1}{\sqrt{B\sqrt{\pi}}} \exp\left[-\frac{(x + D/2)^2}{2B^2}\right] \times \exp\left(\frac{imx^2}{2\hbar R} + i\Delta x + i\theta + i\mu'\right), \quad (24)$$

where

$$B^2(t, \tau) = \frac{\left(\frac{1}{\beta^2} + \frac{1}{b^2}\right)^2 + \frac{m^2}{\hbar^2} \left(\frac{1}{\tau} + \frac{1}{r}\right)^2}{\left(\frac{m}{\hbar\tau}\right)^2 \left(\frac{1}{\beta^2} + \frac{1}{b^2}\right)}, \quad (25)$$

$$R(t, \tau) = \tau \frac{\left(\frac{1}{\beta^2} + \frac{1}{b^2}\right)^2 + \frac{m^2}{\hbar^2} \left(\frac{1}{\tau} + \frac{1}{r}\right)^2}{\frac{1}{\beta^4} + \frac{C}{\sigma_0^4(t^2 + \tau_0^2 + 2\tau_0 t \gamma + t^2 \gamma^2)}}, \quad (26)$$

$$C = \left[\tau_0^2 + \frac{t\tau_0^2}{\tau} + \tau_0^2\gamma^2 + \frac{\tau_0^3\gamma}{\tau} + \frac{t\tau_0^2\gamma^2}{\tau} + \frac{2\tau_0^2\sigma_0^2}{\beta}\right], \quad (27)$$

$$\Delta(t, \tau) = \frac{\tau \sigma_0^2 d}{2\tau_0 \beta^2 B^2}, \quad (28)$$

$$D(t, \tau) = d \frac{\left(1 + \frac{\tau}{r}\right)}{\left(1 + \frac{\beta^2}{b^2}\right)}, \quad (29)$$

$$\theta(t, \tau) = \frac{md^2 \left(\frac{1}{\tau} + \frac{1}{r}\right)}{8\hbar\beta^4 \left[\left(\frac{1}{\beta^2} + \frac{1}{b^2}\right)^2 + \frac{m^2}{\hbar^2} \left(\frac{1}{\tau} + \frac{1}{r}\right)^2\right]}, \quad (30)$$

and

$$\mu'(t, \tau) = -\frac{1}{2} \arctan \left[\frac{t + \tau \left(1 + \frac{\sigma_0^2}{\beta^2} + \frac{t\hbar\gamma}{m\beta^2}\right)}{\tau_0 \left(1 - \frac{t\tau\sigma_0^2}{\tau_0\beta^2}\right) + \gamma(t + \tau)} \right]. \quad (31)$$

The parameter $B(t, \tau)$ is the beam width for the propagation through one slit, $R(t, \tau)$ is the radius of curvature of the wavefronts for the propagation through one slit, $D(t, \tau)$ is the separation between the wavepackets produced in the double-slit. $\Delta(t, \tau)x$ is a phase that varies linearly with the transverse coordinate. $\theta(t, \tau)$ and $\mu'(t, \tau)$ are the time-dependent phases and they are relevant only if the slits have different widths. $\mu'(t, \tau)$ is the Gouy phase for the propagation through one slit. Differently from the results obtained in Ref. [46], all the parameters above are affected by the correlation parameter γ . For the left slit $2(-)$, we have just to substitute the parameter d with $-d$ in the expressions corresponding to the wave passing through the first slit.

Having obtained the wavefunctions, we calculate the cross-Wigner transform. First, we calculate the cross-Wigner between the states $\psi_1(x, t, \tau)$ and $\psi_2(x, t, \tau)$ at the detection screen. It is given by

$$CW_{\psi_1, \psi_2}(x, k) = \frac{1}{2\pi} \int_{-\infty}^{\infty} dy e^{-iky} \psi_1^* \left(x + \frac{y}{2}\right) \psi_2 \left(x - \frac{y}{2}\right),$$

After some algebraic manipulation, we obtain for the real and imaginary parts the following results

$$\begin{aligned} \text{Re}[CW]_{\psi_1, \psi_2}(x, k) &= \frac{2}{\pi} \exp \left[-\left(\frac{x^2}{B^2} + \left(k + \frac{mx}{\hbar R}\right)^2 B^2\right) \right] \\ &\times \cos \left[\left(k + \frac{mx}{\hbar R}\right) D - 2\Delta x \right], \end{aligned} \quad (33)$$

and

$$\begin{aligned} \text{Im}[CW]_{\psi_1, \psi_2}(x, k) &= \frac{2}{\pi} \exp \left[-\left(\frac{x^2}{B^2} + \left(k + \frac{mx}{\hbar R}\right)^2 B^2\right) \right] \\ &\times \sin \left[\left(k + \frac{mx}{\hbar R}\right) D - 2\Delta x \right], \end{aligned} \quad (34)$$

The results above are independent of the Gouy phase because both wave functions evolve at the same time with

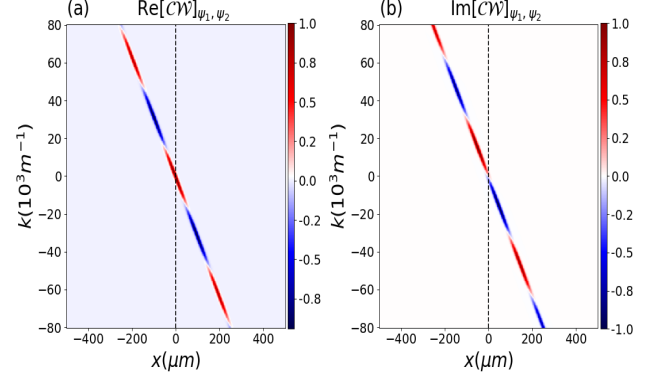


FIG. 4. Normalized cross-Wigner transform (a) Real part ($\text{Re}[CW]_{\psi_1, \psi_2}$) as a function of x and k for $t = 50$ ms, for $\tau = 50$ ms and $\gamma = 0$. The real and imaginary components of the cross-Wigner function only differ by a $\pi/2$ phase. Then, one component can be obtained from the other part through phase displacement in the (x, k) space and (b) the imaginary value ($\text{Im}[CW]_{\psi_1, \psi_2}$) for the same parameters.

respect to the initial state and acquire the same Gouy phase $\mu'(t, \tau)$.

In the following, we consider the neutron parameters $m = 1.67 \times 10^{-27}$ kg, $\sigma_0 = 7.8 \mu\text{m}$, $\beta = 7.8 \mu\text{m}$ and $d = 100 \mu\text{m}$. Fig. 4 shows the plots for the real and imaginary part of the cross-Wigner between the states of propagation through the slits as a function of x and k for $t = 50$ ms, $\tau = 50$ ms, and $\gamma = 0$. The real and imaginary components of the cross-Wigner function only differ by a $\pi/2$ phase, as we can see from Eqs. (33) and (34). Note that the imaginary part can then be obtained from the real part through phase displacement in the (x, k) space.

Next, we calculate the cross-Wigner between the initial state and the state at the detection screen, which is given by

$$(32) \quad CW_{\Psi, \psi_0}(x, k) = \frac{1}{2\pi} \int_{-\infty}^{\infty} dy e^{-iky} \Psi^* \left(x + \frac{y}{2}\right) \psi_0 \left(x - \frac{y}{2}\right), \quad (35)$$

where

$$\Psi(x, t, \tau) = \frac{\psi_1(x, t, \tau) + \psi_2(x, t, \tau)}{\sqrt{2 + 2 \exp \left[-\frac{D^2}{4B^2} - \Delta^2 B^2 \right]}}, \quad (36)$$

is the normalized wave function at the screen of detection of the double-slit experiment. After some algebraic manipulation we obtain for its real and imaginary parts the following results

$$\begin{aligned} \text{Re}[CW]_{\Psi, \psi_0} &= N' e^{-\frac{D^2}{8B^2}} e^{b_1} e^{-b_2 k^2} e^{-b_3 x^2} e^{-b_4 kx} \\ &\times [e^{b_5 x} e^{b_6 k} \cos(\phi_1 + \phi_2) + e^{-b_5 x} e^{-b_6 k} \cos(\phi_1 - \phi_2)], \end{aligned} \quad (37)$$

and

$$\begin{aligned} \text{Im}[\mathcal{CW}]_{\Psi, \psi_0} &= N' e^{-\frac{D^2}{8B^2}} e^{b_1} e^{-b_2 k^2} e^{-b_3 x^2} e^{-b_4 kx} \\ &\times [e^{b_5 x} e^{b_6 k} \sin(\phi_1 + \phi_2) + e^{-b_5 x} e^{-b_6 k} \sin(\phi_1 - \phi_2)], \end{aligned} \quad (38)$$

where

$$\phi_1 = b_7 x^2 + b_8 x + b_9 + b_{10} k^2 - \theta + \Delta\mu', \quad (39)$$

$$\phi_2 = b_{11} x + b_{12} k, \quad (40)$$

and

$$\Delta\mu'(t, \tau) = \xi'(t, \tau) - \mu'(t, \tau) \quad (41)$$

with

$$\xi'(t, \tau) = -\frac{1}{2} \arctan \left(\frac{\frac{m}{2\hbar R} - \frac{\gamma}{2\sigma_0^2}}{\frac{1}{2B^2} + \frac{1}{2\sigma_0^2}} \right). \quad (42)$$

Here, $\Delta\mu'$ is the cross-Wigner Gouy phase difference for the propagation through the slit. The parameters N' and b_i ($i = 1, \dots, 12$) are given in the appendix C. Here we observe that the result is dependent on the cross-Wigner Gouy phase difference $\Delta\mu'(t, \tau)$ because as in the free evolution, the cross-Wigner is calculated for states at different times.

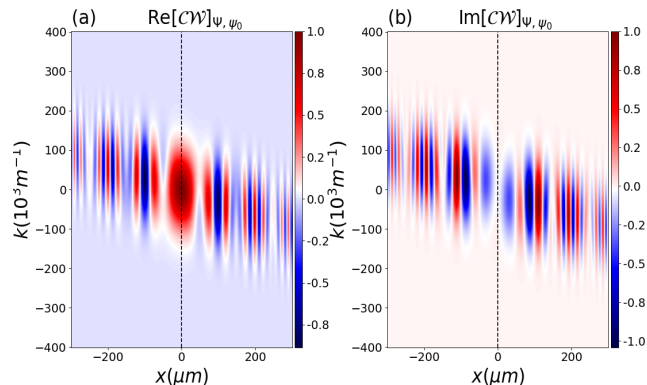


FIG. 5. Normalized cross-Wigner. (a) The real part ($\text{Re}[\mathcal{CW}]_{\Psi, \psi_0}$) as a function of x and k for $t = 50$ ms, for $\tau = 50$ ms and $\gamma = 0$ (b) The imaginary part ($\text{Im}[\mathcal{CW}]_{\Psi, \psi_0}$) with the same parameters .

By considering the same parameters of a wave of neutrons used above we show, in Fig. 5, the cross-Wigner between the initial state and the state at the screen of detection as a function of x and k for $t = 50$ ms, $\tau = 50$ ms and $\gamma = 0$. In (a) we see the normalized cross-Wigner real part from eq.(37) and in (b) imaginary part from eq.(38). Fig. 6 illustrates how the Gouy phase difference affects

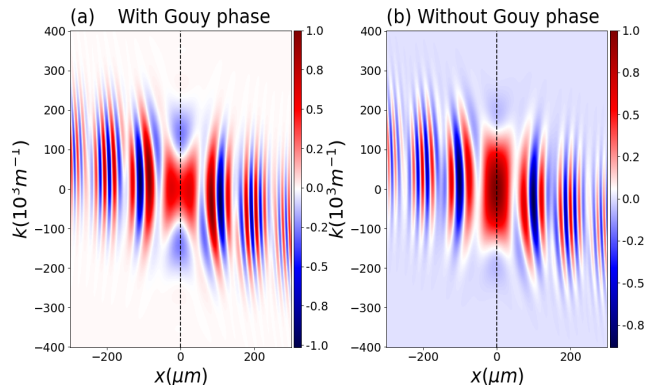


FIG. 6. Normalized cross-Wigner real part ($\text{Re}[\mathcal{CW}]_{\Psi, \psi_0}$) as a function of x and k for $t = 50$ ms, $\tau = 50$ ms and $\gamma = -1$. In (a), we consider the Gouy phase difference, and in (b), we do not consider it. As for the free propagation context, the Gouy phase is crucial for providing a precise and accurate description of the cross-Wigner. We change the value of γ to -1 , in this plot, since the effect is more noticeable than for the case where $\gamma = 0$. We have similar results for the imaginary component.

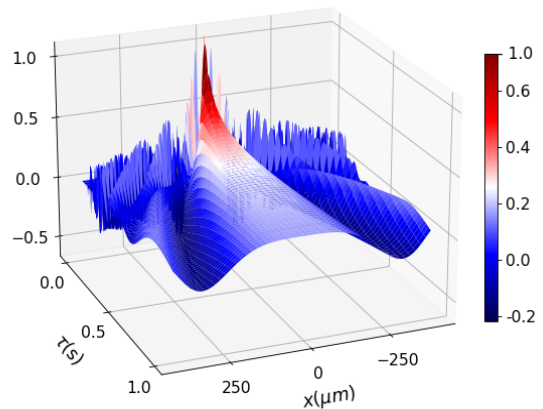


FIG. 7. Normalized cross-Wigner real part ($\text{Re}[\mathcal{CW}]_{\Psi, \psi_0}$) as a function of x and τ for $t = 50$ ms, $k = 0$ and $\gamma = 0$. The cross-Wigner real part in this case exhibits more oscillatory behavior than in the free propagation case, since the state at the detection screen, in this current scenario, is delocalized, characterized by the superposition cat-like state.

the cross-Wigner function's real part and highlights how crucial it is for a precise cross-Wigner description. In this plot, we change the value of γ to -1 since the effect is more noticeable than for the case where $\gamma = 0$ (see appendix A). For the imaginary component, our results are similar.

The normalized cross-Wigner (real part) between the

initial state and the state at the screen of detection as a function of x and τ for $t = 50ms$, $k = 0$ and $\gamma = 0$ is shown in Fig. 7. Compared with Fig. 2, the cross-Wigner real part, in this situation, has more oscillatory behavior than in the free propagation case, since in this current scenario, the state at the detection screen is delocalized, characterized by the superposition cat-like state in eq. (36).

A. Intensity and cross-Wigner reconstruction

In this part, we will show how to reconstruct the cross-Wigner function from an adaption of the currently used techniques to measure the Wigner function. As mentioned before, integrating $W(x, k)$ over k results in

$$I(x) = \int_{-\infty}^{+\infty} W(x, k) dk, \quad (43)$$

which correspond to the interference pattern $I(x) = |\psi_1 + \psi_2|^2$ in the double-slit experiment. If we consider a rotated version of the Wigner function [47], $W_\theta(x, k) = W(x \cos \theta - k \sin \theta, x \sin \theta + k \cos \theta)$, where θ is the angle of rotation in phase-space. This rotated Wigner function results in the following spatial interference pattern

$$I_\theta(x) = \int_{-\infty}^{+\infty} W_\theta(x, k) dk. \quad (44)$$

Inverting the equation (44), the Wigner function can be reconstructed from the continuous set of interference pattern $I_\theta(x)$ through [47, 48]

$$W(x, k) = \frac{1}{4\pi^2} \int_{-\infty}^{+\infty} dx' \int_{-\infty}^{+\infty} |r| dr \times \int_0^\pi d\theta I_\theta(x') e^{ir(x' - x \cos \theta - k \sin \theta)}, \quad (45)$$

know as the inverse Radon transformation [49].

Generally, in optics experiments the balanced homodyne detection technique [50] is used to access the rotated basis ($x' = x \cos \theta + k \sin \theta$; $k' = -x \sin \theta + k \cos \theta$) to obtain the continuous set of interference pattern $I_\theta(x)$. On the other hand, another mechanism for mixing the x and k variables is the free evolution of a particle [51], with the time propagation playing the role of the rotation angle θ . In [51], the authors reconstruct the Wigner function from the interference pattern $I(x, \tau)$ for various propagation times τ from the double-slit to the detection screen.

Since the real part of the cross-Wigner transform is one of the interference terms of the standard Wigner distribution of the sum $\psi_1 + \psi_2$ [36], we can reconstruct the real part of the cross-Wigner function from the interference term $I_{\text{Int}}(x, \tau)$ given by

$$\begin{aligned} I_{\text{Int}}(x, \tau) &= I(x, \tau) - [I_1(x, \tau) + I_2(x, \tau)] \\ &= 2\sqrt{I_1(x, \tau)I_2(x, \tau)} \cos(\Phi_{12}), \end{aligned} \quad (46)$$

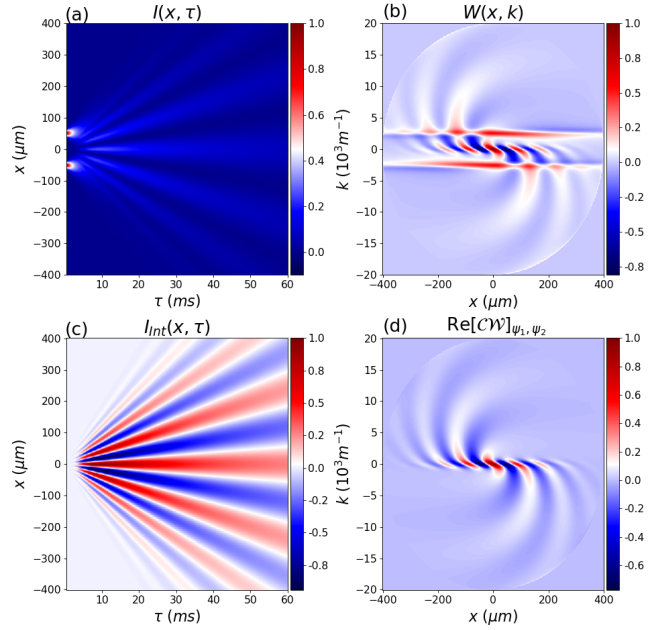


FIG. 8. Cross-Wigner reconstruction procedure. In (a) we represent the interference pattern $I(x, \tau)$ between ψ_1 and ψ_2 in the double-slit experiment for various propagation times τ . (b) Through $I(x, \tau)$ we reconstruct the Wigner function $W(x, k)$. (c) On the other hand, from the interference term $I_{\text{Int}}(x, \tau)$ we obtain the real part of the cross-Wigner ($\text{Re}[\mathcal{CW}]_{\psi_1, \psi_2}$) in (d).

where

$$I_1(x, \tau) = |\psi_1(x, \tau)|^2, \quad I_2(x, \tau) = |\psi_2(x, \tau)|^2, \quad (47)$$

and $\Phi_{12} = 2\Delta x$ is the phase-difference between the states ψ_1 and ψ_2 .

In Fig. 8, we can see how the cross-Wigner reconstruction procedure works. In Fig. 8(a) we represent the interference pattern $I(x, \tau)$ between ψ_1 and ψ_2 in the double-slit experiment for various propagation times τ . As argued in [51], only a limited range of evolution times is available in such an experiment. Then, we should choose an appropriate range of τ , determined by the information on coherence properties of the superposition of the two states ψ_1 and ψ_2 . In Fig. 8(b), through $I(x, \tau)$ we reconstruct the Wigner function $W(x, k)$, where we can see the characteristic Wigner function of Schrodinger cat-like state, with typical Gaussian-like probabilities located at two different regions of phase-space, and between them an additional interference term that can take negative values. In Fig. 8(c), on the other hand, from the interference term $I_{\text{Int}}(x, \tau)$ we obtain the real part of the cross-Wigner ($\text{Re}[\mathcal{CW}]_{\psi_1, \psi_2}$) displayed in Fig. 8(d).

V. CONCLUSIONS

We analyzed in this work the role of the Gouy phase difference, for an accurate and complete description of

the cross-Wigner transform for matter waves characterized by an initially correlated Gaussian wave packet. In contrast to usual wave functions that only present a global Gouy phase, here we discussed that it is relevant for the cross-distribution as it becomes a relative phase in this scenario. Moreover, we showed how the Gouy phase is affected by starting the evolution with initial position-momentum correlations that can also amplify the temporal interference between both wave functions.

We have examined the cross-Wigner between the initial state and the free-evolved one, as well as the evolution through the double-slit arrangement. A temporal Gouy phase difference results from the fact that the cross-Wigner is calculated for wave functions at different times, i.e., $\psi(x, t)$ at the time $t > 0$ and ψ_0 at the time $t = 0$. Then, the cross-Wigner transform provides an interesting tool to assess temporal interference effects. We observe that the phase effect is highlighted when the initial state is contractive because it works as a squeezing agent in this condition, increasing further the transverse confinement of the wavepacket with respect to its propagation direction. We also suggest a method for reconstructing the cross-Wigner function, fully compatible with current experimental technology [51], from the intensity interference term in a double-slit experiment, unveiling then, a relationship between this function and observed physical quantities for matter-waves.

Based on the results discussed here, one natural extension of this method can be employed to reconstruct cross-Wigner functions with different times of propagation. This idea can be worked on by introducing interferometers like the Franson time interference fringes and temporal beam-splitters [52] since a sequence of time refraction processes is shown to lead to temporal interference effects. With that, we can then produce interference at the output and use it to reconstruct the cross-Wigner transform.

It is noteworthy that the Franson interferometer was employed to provide security in a protocol for large-alphabet quantum key distribution [53], where energy-time entanglement is shown to be robust to transmission over large distances in optical fiber. To this end, our work suggests that cross-Wigner formalism could provide new insights for these applications. We let this reconstruction, as well as some possible interesting connections with weak values and cryptography to future investigation.

ACKNOWLEDGMENTS

L.S.M. acknowledges Fundação de Amparo à Ciência e Tecnologia do Estado de Pernambuco and Office of Naval Research (N62909-23-1-2014). P.R.D. acknowledges support from the Foundation for Polish Science (IRAP project, ICTQT, Contract No. MAB/2018/5, co-financed by EU within Smart Growth Operational Programme). C.H.S.V. acknowledges CAPES (Brazil) and Federal University of ABC for the financial sup-

port. I.G.P. acknowledges Grant No. 306528/[2023-1] from CNPq.

Appendix A: Gouy phase behavior with correlation parameter

This appendix shows that the time behavior of the Gouy phase is more pronounced for some values of the correlation parameter. In this setting, the Gouy phase is even more important for an accurate description of the Cross-Wigner function.

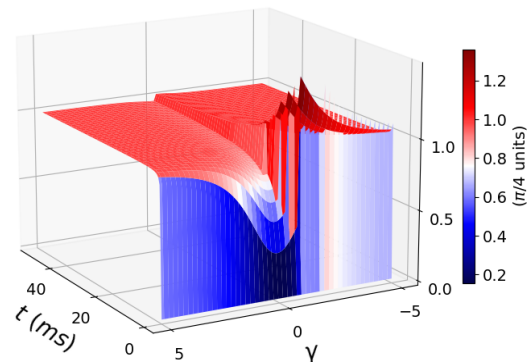


FIG. 9. Absolute value of the Gouy phase difference, for the free evolution case, as a function of γ and t . Note that, the phase effect is more apparent when the state is contractive $\gamma < 0$, increasing further the transverse confinement of the wavepacket with respect to its propagation direction, and consequently, increasing the Gouy phase.

In Fig. 9, we plot the absolute value of the Gouy phase difference, for the free evolution case, as a function of γ and t . The behavior of the Gouy phase difference accumulated throughout the propagation period t can be seen. Moreover, note the dependence with the correlation parameter γ , as expected, since it is responsible for modifying transversely the confinement condition of the wavepacket with respect to its propagation direction [54], causing further phase accumulation for states with $\gamma \neq 0$. It should be noted that the phase effect is even more apparent for $\gamma < 0$, a state known as contractive [55] since it can be viewed as a squeezing agent in this case [54]. However, when $\gamma > 0$, the result is the opposite.

We plot, in Fig. 10, the cross-Wigner Gouy phase difference, for evolution through a double-slit, as a function γ and τ for $t = 50$ ms. We observe the behavior of the Gouy phase difference acquired during the propagation time τ . The additional phase accumulation is again dependent on the correlation parameter, just as in the free-propagation case. Notice that there are some values of γ where the phase effect is more pronounced than oth-

ers, indicating specific settings where the phase is more important.

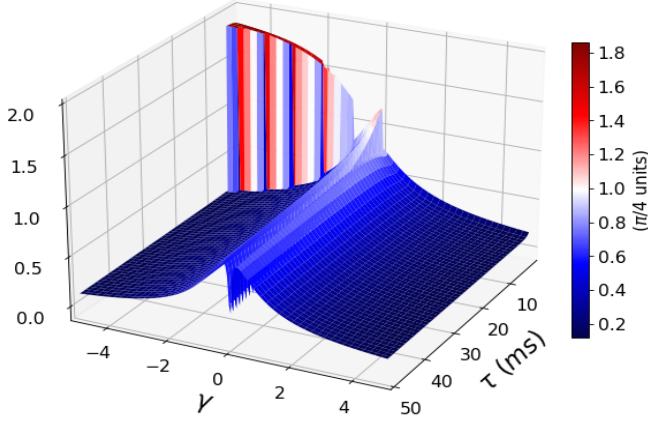


FIG. 10. Absolute value of the Gouy phase difference, for evolution through a double-slit, as a function γ and τ for $t = 50$ ms. The additional phase accumulation is influenced by the correlation parameter again, similar to the free-propagation scenario. For some values of γ , the phase has a greater magnitude, indicating specific settings where the phase effect is more evident.

Appendix B: Parameters of the cross-Wigner for free evolution

Here, we describe the parameters used to construct the real and imaginary parts of the cross-Wigner function while considering the free-evolution of a correlated Gaussian state (eq. (11)) and the initial state (eq. (8)), as shown in the main text.

$$A = \left(\frac{1}{2b^2} + \frac{1}{2\sigma_0^2} \right)^2 + \left(\frac{m}{2\hbar r} - \frac{\gamma}{2\sigma_0^2} \right)^2, \quad (\text{B1})$$

$$N^{-1} = \pi \sqrt{b\sigma_0}^4 \sqrt{\left(\frac{1}{2b^2} + \frac{1}{2\sigma_0^2} \right)^2 + \left(\frac{m}{2\hbar r} - \frac{\gamma}{2\sigma_0^2} \right)^2}, \quad (\text{B2})$$

$$a_1 = \left(\frac{1}{2b^2} + \frac{1}{2\sigma_0^2} \right) - a_{11}, \quad (\text{B3})$$

$$a_2 = - \left(\frac{m}{2\hbar r} - \frac{\gamma}{2\sigma_0^2} \right) + a_{22}, \quad (\text{B4})$$

$$a_3 = \frac{1}{A} \left(\frac{1}{2b^2} + \frac{1}{2\sigma_0^2} \right), \quad (\text{B5})$$

$$a_4 = \frac{1}{A} \left(\frac{m}{2\hbar r} - \frac{\gamma}{2\sigma_0^2} \right), \quad (\text{B6})$$

$$a_5 = \frac{2}{A} \left(\frac{1}{2b^2} - \frac{1}{2\sigma_0^2} \right) \left(\frac{m}{2\hbar r} - \frac{\gamma}{2\sigma_0^2} \right) - \frac{2}{A} \left(\frac{m}{2\hbar r} + \frac{\gamma}{2\sigma_0^2} \right) \left(\frac{1}{2b^2} + \frac{1}{2\sigma_0^2} \right), \quad (\text{B7})$$

$$a_6 = \frac{2}{A} \left(\frac{m}{2\hbar r} + \frac{\gamma}{2\sigma_0^2} \right) \left(\frac{m}{2\hbar r} - \frac{\gamma}{2\sigma_0^2} \right) + \frac{2}{A} \left(\frac{1}{2b^2} - \frac{1}{2\sigma_0^2} \right) \left(\frac{1}{2b^2} + \frac{1}{2\sigma_0^2} \right), \quad (\text{B8})$$

$$a_{11} = \frac{1}{A} \left[\left(\frac{1}{2b^2} - \frac{1}{2\sigma_0^2} \right)^2 - \left(\frac{m}{2\hbar r} + \frac{\gamma}{2\sigma_0^2} \right)^2 \right] \times \left(\frac{1}{2b^2} + \frac{1}{2\sigma_0^2} \right) \quad (\text{B9})$$

$$+ \frac{2}{A} \left(\frac{1}{2b^2} - \frac{1}{2\sigma_0^2} \right) \left(\frac{m}{2\hbar r} + \frac{\gamma}{2\sigma_0^2} \right) \left(\frac{m}{2\hbar r} - \frac{\gamma}{2\sigma_0^2} \right),$$

$$a_{22} = -\frac{1}{A} \left[\left(\frac{1}{2b^2} - \frac{1}{2\sigma_0^2} \right)^2 - \left(\frac{m}{2\hbar r} + \frac{\gamma}{2\sigma_0^2} \right)^2 \right] \times \left(\frac{m}{2\hbar r} + \frac{\gamma}{2\sigma_0^2} \right) \quad (\text{B10})$$

$$+ \frac{2}{A} \left(\frac{1}{2b^2} - \frac{1}{2\sigma_0^2} \right) \left(\frac{1}{2b^2} + \frac{1}{2\sigma_0^2} \right) \left(\frac{m}{2\hbar r} + \frac{\gamma}{2\sigma_0^2} \right).$$

Appendix C: Parameters of the cross-Wigner for evolution through a double-slit

In this part, we present the parameters that were utilized to describe the real and imaginary parts of the cross-Wigner function between the initial state (eq. (8)) and the superposition state at the detection screen (eq. (36)).

$$A' = \left(\frac{1}{2B^2} + \frac{1}{2\sigma_0^2} \right)^2 + \left(\frac{m}{2\hbar R} - \frac{\gamma}{2\sigma_0^2} \right)^2 \quad (\text{C1})$$

$$N'^{-1} = \pi \sqrt{B\sigma_0}^4 \sqrt{A'} \sqrt{2 + 2 \exp \left[-\frac{D^2}{4B^2} - \Delta^2 B^2 \right]}, \quad (\text{C2})$$

$$\alpha_1 = \frac{1}{A'} \left[\left(\frac{1}{4B^4} - \frac{1}{4\sigma_0^4} \right) + 2 \left(\frac{m^2}{4\hbar^2 R^2} - \frac{\gamma^2}{4\sigma_0^4} \right) \right] \times \left(\frac{1}{2B^2} - \frac{1}{2\sigma_0^2} \right) - \frac{1}{A'} \left(\frac{m}{2\hbar R} + \frac{\gamma}{2\sigma_0^2} \right) \left(\frac{1}{2B^2} + \frac{1}{2\sigma_0^2} \right) \quad (\text{C3})$$

$$\alpha_2 = -\frac{1}{A'} \left[\left(\frac{1}{2B^2} - \frac{1}{2\sigma_0^2} \right)^2 - \left(\frac{m}{2\hbar R} + \frac{\gamma}{2\sigma_0^2} \right)^2 \right] \\ \times \left(\frac{m}{2\hbar R} - \frac{\gamma}{2\sigma_0^2} \right) + \frac{2}{A'} \left(\frac{m}{2\hbar R} + \frac{\gamma}{2\sigma_0^2} \right) \left(\frac{1}{4B^4} - \frac{1}{4\sigma_0^4} \right) \quad (\text{C4})$$

$$b_1 = \frac{1}{A'} \left(\frac{D^2}{16B^4} - \frac{\Delta^2}{4} \right) \left(\frac{1}{2B^2} + \frac{1}{2\sigma_0^2} \right) \\ + \left(\frac{m}{2\hbar R} - \frac{\gamma}{2\sigma_0^2} \right) \left(\frac{\Delta D}{4B^2 A'} \right) \quad (\text{C5})$$

$$b_2 = \frac{1}{A'} \left(\frac{1}{2B^2} + \frac{1}{2\sigma_0^2} \right) \quad (\text{C6})$$

$$b_3 = \frac{1}{2B^2} + \frac{1}{2\sigma_0^2} - \alpha_1 \quad (\text{C7})$$

$$b_4 = \frac{1}{A'} \left(\frac{m}{\hbar R \sigma_0^2} + \frac{\gamma}{\sigma_0^2 B^2} \right) \quad (\text{C8})$$

$$b_5 = \left[\left(\frac{1}{4B^4} - \frac{1}{4\sigma_0^4} \right) + \left(\frac{m^2}{4\hbar^2 R^2} - \frac{\gamma^2}{4\sigma_0^4} \right) \right] \left(\frac{D}{2B^2 A'} \right) \\ - \frac{\Delta}{2A'} \left(\frac{m}{\hbar R \sigma_0^2} + \frac{\gamma}{\sigma_0^2 B^2} \right) - \frac{D}{2B^2} \quad (\text{C9})$$

$$b_6 = \left(\frac{m}{2\hbar R} - \frac{\gamma}{2\sigma_0^2} \right) \left(\frac{D}{2B^2 A'} \right) - \left(\frac{1}{2B^2} + \frac{1}{2\sigma_0^2} \right) \left(\frac{\Delta}{A'} \right) \quad (\text{C10})$$

$$b_7 = \alpha_2 - \frac{m}{2\hbar R} + \frac{\gamma}{2\sigma_0^2} \quad (\text{C11})$$

$$b_8 = \frac{1}{A'} \left[\left(\frac{1}{2B^4} - \frac{1}{2\sigma_0^4} \right) + \left(\frac{m^2}{2\hbar^2 R^2} - \frac{\gamma^2}{2\sigma_0^4} \right) \right] \quad (\text{C12})$$

$$b_9 = \frac{1}{A'} \left(-\frac{D^2}{16B^4} + \frac{\Delta^2}{4} \right) \left(\frac{m}{2\hbar R} - \frac{\gamma}{2\sigma_0^2} \right) \\ + \left(\frac{1}{2B^2} + \frac{1}{2\sigma_0^2} \right) \left(\frac{\Delta D}{4B^2 A'} \right) \quad (\text{C13})$$

$$b_{10} = \frac{1}{A'} \left(\frac{m}{2\hbar R} - \frac{\gamma}{2\sigma_0^2} \right) \quad (\text{C14})$$

$$b_{11} = \frac{\Delta}{2A'} \left[\left(\frac{1}{2B^4} - \frac{1}{2\sigma_0^4} \right) + \left(\frac{m^2}{4\hbar^2 R^2} - \frac{\gamma^2}{2\sigma_0^4} \right) \right] \\ + \left(\frac{m}{2\hbar R \sigma_0^2} + \frac{\gamma}{2\sigma_0^2 B^2} \right) \left(\frac{D}{2B^2 A'} \right) - \Delta \quad (\text{C15})$$

$$b_{12} = \left(\frac{1}{2B^2} + \frac{1}{2\sigma_0^2} \right) \left(\frac{D}{2B^2 A'} \right) \\ + \left(\frac{m}{2\hbar R} - \frac{\gamma}{2\sigma_0^2} \right) \left(\frac{\Delta}{A'} \right) \quad (\text{C16})$$

-
- [1] L. G. Gouy, *Sur une propriété nouvelle des ondes lumineuses* (Gauthier-Villars, 1890).
- [2] L. G. Gouy, *Sur la propagation anormale des ondes*, *Compt. Rendue Acad. Sci. Paris* **111**, 33 (1890).
- [3] I. G. da Paz, M. C. Nemes, and J. G. P. de Faria, Gouy phase and matter waves, *Journal of Physics: Conference Series* **84**, 012016 (2007).
- [4] I. G. da Paz, M. C. Nemes, S. Pádua, C. H. Monken, and J. G. P. de Faria, Indirect evidence for the Gouy phase for matter waves, *Phys. Lett. A* **374**, 1660 (2010).
- [5] I. Da Paz, P. Saldanha, M. Nemes, and J. P. De Faria, Experimental proposal for measuring the gouy phase of matter waves, *New J. Phys.* **13**, 125005 (2011).
- [6] A. Hansen, J. T. Schultz, and N. P. Bigelow, Measuring the gouy phase of matter waves using full bloch bose-einstein condensates, in *The Rochester Conferences on Coherence and Quantum Optics and the Quantum Information and Measurement meeting* (Optica Publishing Group, 2013) p. M6.64.
- [7] X. Pang, T. D. Visser, and E. Wolf, Phase anomaly and phase singularities of the field in the focal region of high-numerical aperture systems, *Opt. Comm.* **284**, 5517 (2011).
- [8] X. Pang, G. Gbur, and T. D. Visser, The gouy phase of airy beams, *Opt. Lett.* **36**, 2492 (2011).

- [9] X. Pang and T. D. Visser, Manifestation of the gouy phase in strongly focused, radially polarized beams, *Opt. Exp.* **21**, 8331 (2013).
- [10] X. Pang, D. G. Fischer, and T. D. Visser, Wavefront spacing and gouy phase in presence of primary spherical aberration, *Opt. Lett.* **39**, 88 (2014).
- [11] S. Feng and H. G. Winful, Physical origin of the gouy phase shift, *Opt. Lett.* **26**, 485 (2001).
- [12] C. Ferreira, L. Marinho, T. Brazil, L. Cabral, J. de Oliveira Jr, M. Sampaio, and I. da Paz, Gouy phase and visibility in the double-slit experiment, *Ann. of Phys.* **362**, 473 (2015).
- [13] N. Holme, M. Myaing, and T. Norris, Gouy phase shift of single-cycle picosecond acoustic pulses, in *The Thirteenth International Conference on Ultrafast Phenomena* (Optica Publishing Group, 2002) p. ThA5.
- [14] D. Chauvat, O. Emile, M. Brunel, and A. Le Floch, Huygens' principle and young's experiment in the propagation of light beams, *Am. J. Phys.* **71**, 1196 (2003).
- [15] M. C. Kobold and P.-P. J. Beaujean, Acoustic error approximation due to Gouy phase in the sea, *AIP Advances* **13**, 075310 (2023), https://pubs.aip.org/aip/adv/article-pdf/doi/10.1063/5.0154593/18037826/075310_1.5.0154593.pdf.
- [16] W. Zhu, A. Agrawal, and A. Nahata, Direct measurement of the gouy phase shift for surface plasmon-polaritons, *Opt. Exp.* **15**, 9995 (2007).
- [17] J. T. Schultz, A. Hansen, and N. P. Bigelow, A raman waveplate for spinor bose-einstein condensates, *Opt. Lett.* **39**, 4271 (2014).
- [18] G. Guzzinati, P. Schattschneider, K. Y. Bliokh, F. Nori, and J. Verbeeck, Observation of the larmor and gouy rotations with electron vortex beams, *Phys. Rev. Lett.* **110**, 093601 (2013).
- [19] P. Schattschneider, T. Schachinger, M. Stöger-Pollach, S. Löffler, A. Steiger-Thirsfeld, K. Y. Bliokh, and F. Nori, Imaging the dynamics of free-electron landau states, *Nat. Comm.* **5**, 4586 (2014).
- [20] T. Petersen, D. Paganin, M. Weyland, T. P. Simula, S. A. Eastwood, and M. J. Morgan, Measurement of the gouy phase anomaly for electron waves, *Phys. Rev. A* **88**, 043803 (2013).
- [21] M. Hiekkämäki, R. F. Barros, M. Ornigotti, and R. Fickler, Observation of the quantum gouy phase, *Nature Photonics* **16**, 828 (2022).
- [22] A. E. Siegman, *Lasers* (University science books, 1986).
- [23] P. Balcou and A. L'Huillier, Phase-matching effects in strong-field harmonic generation, *Phys. Rev. A* **47**, 1447 (1993).
- [24] M. Lewenstein, P. Salieres, and A. L'huillier, Phase of the atomic polarization in high-order harmonic generation, *Phys. Rev. A* **52**, 4747 (1995).
- [25] F. Lindner, W. Stremme, M. G. Schätzel, F. Grasbon, G. G. Paulus, H. Walther, R. Hartmann, and L. Strüder, High-order harmonic generation at a repetition rate of 100 khz, *Phys. Rev. A* **68**, 013814 (2003).
- [26] F. Lindner, G. G. Paulus, H. Walther, A. Baltuška, E. Goulielmakis, M. Lezius, and F. Krausz, Gouy phase shift for few-cycle laser pulses, *Phys. Rev. Lett.* **92**, 113001 (2004).
- [27] L. Allen, M. W. Beijersbergen, R. Spreeuw, and J. Woerdman, Orbital angular momentum of light and the transformation of laguerre-gaussian laser modes, *Phys. Rev. A* **45**, 8185 (1992).
- [28] L. Allen, M. Padgett, and M. Babiker, Iv the orbital angular momentum of light, in *Prog. Opt.*, Vol. 39 (Elsevier, 1999) pp. 291–372.
- [29] Y. Guo, V. D. Vaidya, R. M. Kroeze, R. A. Lunney, B. L. Lev, and J. Keeling, Emergent and broken symmetries of atomic self-organization arising from gouy phase shifts in multimode cavity qed, *Phys. Rev. A* **99**, 053818 (2019).
- [30] B. P. da Silva, V. Pinillos, D. Tasca, L. Oxman, and A. Khoury, Pattern revivals from fractional gouy phases in structured light, *Phys. Rev. Lett.* **124**, 033902 (2020).
- [31] X. Gu, M. Krenn, M. Erhard, and A. Zeilinger, Gouy phase radial mode sorter for light: Concepts and experiments, *Phys. Rev. Lett.* **120**, 103601 (2018).
- [32] I. Da Paz, C. Vieira, R. Ducharme, L. Cabral, H. Alexander, and M. Sampaio, Gouy phase in nonclassical paths in a triple-slit interference experiment, *Phys. Rev. A* **93**, 033621 (2016).
- [33] F. R. Lustosa, P. R. Dieguez, and I. G. da Paz, Irrealism from fringe visibility in matter-wave double-slit interference with initial contractive states, *Phys. Rev. A* **102**, 052205 (2020).
- [34] L. Cohen, *Time-frequency analysis*, Vol. 778 (Prentice hall New Jersey, 1995).
- [35] L. Cohen and P. Loughlin, leid1. time-frequency analysis: Theory and applications, *J. Acous. Soc. Ame.* **134**, 4002 (2013).
- [36] M. A. de Gosson and S. M. de Gosson, Weak values of a quantum observable and the cross-Wigner distribution, *Phys. Lett. A* **376**, 293 (2012).
- [37] M. A. de Gosson and S. M. de Gosson, The reconstruction problem and weak quantum values, *J. Phys. A: Math. Theor.* , 115305 (2012).
- [38] Y. Aharonov, P. G. Bergmann, and J. L. Lebowitz, Time symmetry in the quantum process of measurement, *Phys. Rev.* **134**, B1410 (1964).
- [39] J. D. Franson, Bell inequality for position and time, *Phys. Rev. Lett.* **62**, 2205 (1989).
- [40] C. Chen, J. H. Shapiro, and F. N. C. Wong, Experimental demonstration of conjugate-franson interferometry, *Phys. Rev. Lett.* **127**, 093603 (2021).
- [41] R. Tirole, S. Vezzoli, E. Galiffi, I. Robertson, D. Maurice, B. Tilmann, S. A. Maier, J. B. Pendry, and R. Sapienza, Double-slit time diffraction at optical frequencies, *Nature Physics* **19**, 999 (2023).
- [42] T. Kaneyasu, Y. Hikosaka, S. Wada, M. Fujimoto, H. Ota, H. Iwayama, and M. Katoh, Time domain double slit interference of electron produced by xuv synchrotron radiation, *Scientific Reports* **13**, 6142 (2023).
- [43] V. Dodonov, Nonclassical'states in quantum optics: asqueezed'review of the first 75 years, *J. Opt. B: Quantum Semiclass. Opt.* **4**, R1 (2002).
- [44] V. Dodonov and A. Dodonov, Transmission of correlated gaussian packets through a delta-potential, *Russ. Laser Res.* **35**, 39 (2014).
- [45] G. Glionna, A. H. Blin, B. Hiller, M. C. Nemes, M. Sampaio, and A. F. R. de Toledo Piza, Dispersion and uncertainty in multislit matter wave diffraction, *Physica A* **387**, 1485 (2008).
- [46] J. S. M. Neto, L. A. Cabral, and I. G. da Paz, Position-momentum correlations in matter waves double-slit experiment, *Eur. J. Phys.* **36**, 035002 (2015).
- [47] U. Janicke and M. Wilkens, Tomography of atom beams, *Journal of Modern Optics* **42**, 2183 (1995), <https://doi.org/10.1080/09500349514551901>.

- [48] K. Vogel and H. Risken, Determination of quasiprobability distributions in terms of probability distributions for the rotated quadrature phase, *Phys. Rev. A* **40**, 2847 (1989).
- [49] G. T. Herman, *Fundamentals of Computerized Tomography: Image Reconstruction from Projections* (Spring - 2 ed., (2009)).
- [50] A. I. Lvovsky, H. Hansen, T. Aichele, O. Benson, J. Mlynek, and S. Schiller, Quantum state reconstruction of the single-photon fock state, *Phys. Rev. Lett.* **87**, 050402 (2001).
- [51] C. Kurtsiefer, T. Pfau, and J. Mlynek, Measurement of the wigner function of an ensemble of helium atoms, *Nature* **386**, 150 (1997).
- [52] J. Mendonça, A. Martins, and A. Guerreiro, Temporal beam splitter and temporal interference, *Physical Review A* **68**, 043801 (2003).
- [53] I. Ali-Khan, C. J. Broadbent, and J. C. Howell, Large-alphabet quantum key distribution using energy-time entangled bipartite states, *Phys. Rev. Lett.* **98**, 060503 (2007).
- [54] L. S. Marinho, I. G. da Paz, and M. Sampaio, Squeezing and slowed quantum decoherence in the double-slit experiment, *Phys. Rev. A* **101**, 062109 (2020).
- [55] H. P. Yuen, Contractive states and the standard quantum limit for monitoring free-mass positions, *Phys. Rev. Lett.* **51**, 719 (1983).

Author contributions L.S.M., P.R.D., C.H.S.V. and I.G.P. contributed equally for the calculations and for writing the manuscript. All authors read and approved the final manuscript.

Competing interests Te authors declare no competing interests.

Additional information Correspondence and requests for materials should be addressed to L.S.M

Data availability

The datasets used and/or analysed during the current study available from the corresponding author on reasonable request.